HHFW Heating and Current Drive Studies of NSTX H-Mode Plasmas

G. Taylor[a], P. T. Bonoli[b], D. L. Green[c], R. W. Harvey[d], J. C. Hosea[a], E. F. Jaeger[c], B. P. LeBlanc[a], R. Maingi[c], C. K. Phillips[a], P. M. Ryan[c], E. J. Valeo[a], J. R. Wilson[a], J. C. Wright[b], and the NSTX Team[a]

[a]*Princeton Plasma Physics Laboratory, Princeton, New Jersey 08543, USA*
[b]*MIT Plasma Science and Fusion Center, Cambridge, Massachusetts 02139, USA*
[c]*Oak Ridge National Laboratory, Oak Ridge, Tennessee 37831, USA*
[d]*CompX, PO Box 2672, Del Mar, California 92014, USA*

Abstract. 30 MHz high-harmonic fast wave (HHFW) heating and current drive are being developed to assist fully non-inductive plasma current (I_p) ramp-up in NSTX. The initial approach to achieving this goal has been to heat I_p = 300 kA inductive plasmas with current drive antenna phasing in order to generate an HHFW H-mode with significant bootstrap and RF-driven current. Recent experiments, using only 1.4 MW of RF power (P_{RF}), achieved a non-inductive current fraction, $f_{NI} \sim 0.65$. Improved antenna conditioning resulted in the generation of I_p = 650 kA HHFW H-mode plasmas, with $f_{NI} \sim 0.35$, when $P_{RF} \geq 2.5$ MW. These plasmas have little or no edge localized mode (ELM) activity during HHFW heating, a substantial increase in stored energy and a sustained central electron temperature of 5-6 keV. Another focus of NSTX HHFW research is to heat an H-mode generated by 90 keV neutral beam injection (NBI). Improved HHFW coupling to NBI-generated H-modes has resulted in a broad increase in electron temperature profile when HHFW heating is applied. Analysis of a closely matched pair of NBI and HHFW+NBI H-mode plasmas revealed that about half of the antenna power is deposited inside the last closed flux surface (LCFS). Of the power damped inside the LCFS about two-thirds is absorbed directly by electrons and one-third accelerates fast-ions that are mostly promptly lost from the plasma. At longer toroidal launch wavelengths, HHFW+NBI H-mode plasmas can have an RF power flow to the divertor outside the LCFS that significantly reduces RF power deposition to the core. ELMs can also reduce RF power deposition to the core and increase power deposition to the edge. Recent full wave modeling of NSTX HHFW+NBI H-mode plasmas, with the model extended to the vessel wall, predicts a coaxial standing mode between the LCFS and the wall that can have large amplitudes at longer launch wavelengths. These simulation results qualitatively agree with HHFW+NBI H-mode data that show decreasing core RF heating efficiency and increasing RF power flow to the lower divertor at longer launch wavelengths.

Keywords: **Spherical Torus, RF Heating and Current Drive.**
PACS: 52.50.Qt, 52.55.Fa, 52.55.Wq

INTRODUCTION

In order for the spherical torus (ST) to be a viable nuclear fusion device it is necessary to eliminate the need for the central solenoid. It is therefore important to develop plasma scenarios that are fully non-inductive. High-harmonic fast wave (HHFW) radio-frequency (RF) power can be used in ST devices to efficiently heat

electrons [1], generating significant bootstrap and RF-driven currents. The HHFW heating system on National Spherical Torus Experiment (NSTX) has a 12-strap antenna array covering about one quarter of the toroidal midplane that is fed by six decoupled RF sources operating at 30 MHz. This antenna design provides good spectral selectivity over a wide range of launch wavelengths corresponding to toroidal wavenumbers (k_ϕ) between ±3 and ±14 m^{-1} [2-4]. In 2009, the single-feed, end-grounded antenna straps were replaced with double-feed, center-grounded straps to reduce the RF electric fields in the vicinity of the Faraday shield for a given strap current. The experimental results presented in this paper were obtained with this new double-feed antenna configuration, together with extensive vacuum and plasma RF conditioning, and by using lithium conditioning to reduce the edge density [5].

In NSTX HHFW heating and current drive are required for non-inductive ramp-up of the plasma current (I_p) to 400-500 kA, where the 90 keV neutral beam injection (NBI) ions can be confined. The initial approach to achieving this goal has been to heat relatively low I_p (~ 300 kA) inductive plasmas with current drive antenna phasing in order to generate an HHFW H-mode with significant bootstrap and RF-driven currents. Through improved plasma and antenna conditioning HHFW H-mode plasmas have been initiated and sustained at I_p = 300 - 650 kA. These plasmas have non-inductive current fractions, f_{NI} ~ 0.65 at I_p = 300 kA when using only 1.4 MW of RF power (P_{RF}) and should achieve $f_{NI} \geq 1$ with P_{RF} ~ 3 MW, well below the maximum arc-free RF power coupled to plasmas in NSTX so far. Another role of HHFW power in NSTX is to provide bulk electron heating in NBI H-mode plasmas. Improved antenna conditioning has resulted in NBI+HHFW H-mode plasmas that show a broad increase in the electron temperature profile when RF power is applied. Significant RF power flows to the divertor are both observed and modeled during HHFW+NBI H-mode plasmas. In this paper we present recent experimental and modeling results for NSTX HHFW and HHFW+NBI H-mode plasmas.

HHFW-GENERATED H-MODE PLASMAS

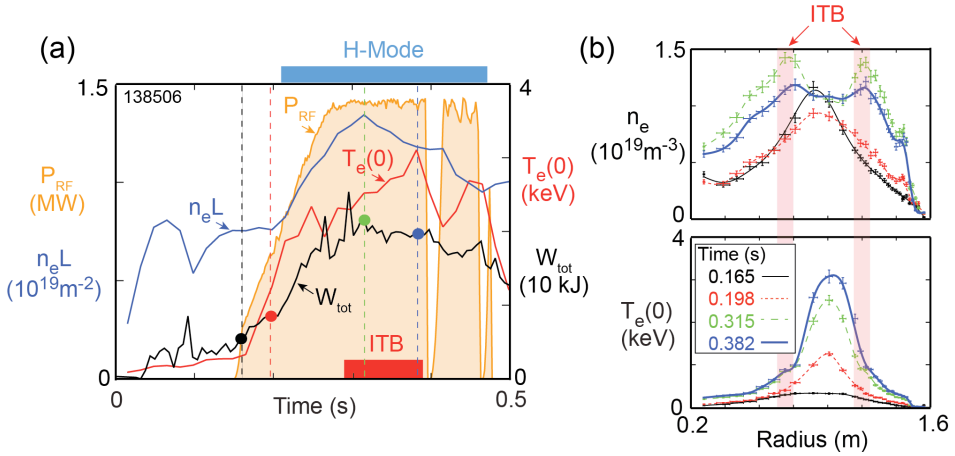

FIGURE 1. (a) Time evolution of n_eL, $T_e(0)$, W_{tot} and P_{RF} for an I_p = 300 kA, $B_T(0)$ = 5.5 kG HHFW deuterium H-mode (shot 138506) using k_ϕ = -8 m^{-1} RF heating. (b) n_e and T_e profiles show the development of an H-mode pedestal as the RF power is ramped up and eventually the formation of an internal transport barrier (ITB).

Recent experiments using only 1.4 MW of k_φ = -8 m^{-1} RF power (P_{RF}) achieved f_{NI} ~ 0.65. Figure 1(a) shows the time evolution of the line integral electron density (n_eL), the central electron temperature ($T_e(0)$), the plasma stored energy (W_{tot}) and P_{RF} for a deuterium plasma with I_p = 300 kA and a toroidal field on the magnetic axis, $B_T(0)$ = 5.5 kG (shot 138506). P_{RF} begins ramping up at 0.15 s, the plasma transitions to a H-mode at 0.21 s, when P_{RF} ~ 1 MW, and an internal transport barrier (ITB) forms at 0.29 s. $T_e(0)$ increases from 0.3 to 3 keV and W_{tot} increases from 5 to 20 kJ during the HHFW heating pulse. The electron density and temperature profiles measured by multi-point Thomson scattering (MPTS) (Fig. 1(b)) show the development of an H-mode pedestal, and eventually the formation of the ITB.

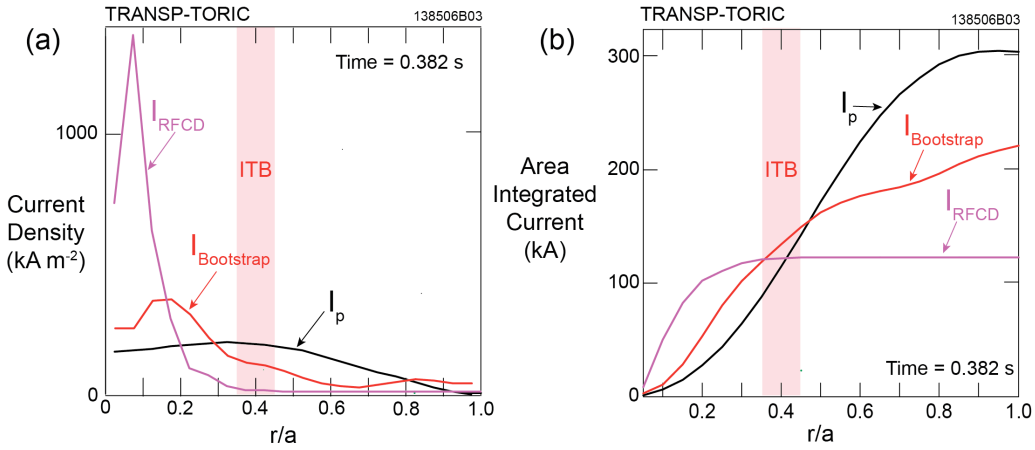

FIGURE 2. TRANSP-TORIC modeling results for shot 138506 at 0.382 s, assuming 100% RF coupling efficiency. (a) Current density profiles and (b) area integrated current, plotted versus normalized minor radius (r/a).

The RF power deposition and current drive profiles for shot 138506 were modeled with a version of the TORIC full-wave code [6] integrated into the TRANSP transport code [7]. Results at 0.382 s are shown in Fig. 2. These results assume an RF coupling efficiency, η_{eff} = 100%. Figure 2(a) shows the profiles of the RF-driven current (I_{RFCD}), the bootstrap current ($I_{Bootstrap}$) and I_p, plotted versus normalized minor radius (r/a). Figure 2(b) shows these current components area integrated and plotted versus r/a. I_{RFCD} is peaked near the magnetic axis and about 60% of $I_{Bootstrap}$ is driven inside the ITB, located at r/a ~ 0.4. As mentioned above these results assume η_{eff} = 100%, an estimate of the actual η_{eff} can be obtained from $\eta_{eff} = \Delta W_{tot}/(\tau * P_{RF})$, where the change in stored energy during RF heating, ΔW_{tot} ~ 13 kJ, P_{RF} = 1.4 MW, and the total energy confinement time, τ ~ 15 ms, yielding η_{eff} ~ 60%. Using this η_{eff}, $I_{Bootstrap}$ ~ 130 kA, I_{RFCD} ~ 70kA, and f_{NI} ~ 0.65. This positive result was achieved by the feedback between the generation of the ITB, the high $T_e(0)$, and a high RF current drive efficiency of, ξ_{cd} ~ 0.1 MA/MW.

Improved antenna conditioning [4, 5] has resulted in HHFW-generated H-mode plasmas at I_p = 650 kA, $B_T(0)$ = 0.55 T, when $P_{RF} \geq$ 2.5 MW. These plasmas have little or no edge localized mode (ELM) activity, a substantial increase in W_{tot} and electron stored energy (W_e), and a sustained $T_e(0)$ = 5-6 keV [8]. Figure 3 summarizes some of the results for a I_p = 650 kA, $B_T(0)$ = 5.5 kG, helium H-mode generated with 2.7 MW of k_φ = -8 m^{-1} RF heating (shot 135260). $T_e(0)$ rapidly increases from 0.5 keV at 0.2 s, when the RF power is turned on, to 6 keV at 0.3 s (Fig. 3(a)), while W_{tot}

increases from 25 kJ to 50 kJ (Fig. 3(b)), with this increase being due almost entirely to a rise in W_e. The plasma remains in L-mode at 0.298 s, as indicated by the peaked $n_e(R)$ plotted in Fig. 3(d). A slow transition to an H-mode with small ELMs begins around 0.37 s and the stored energy rises throughout the remainder of the RF pulse until a large ELM occurs near the end of the pulse. Figure 3(d) shows that the $n_e(R)$ at 0.465 s has developed a steep edge pedestal characteristic of the H-mode and a soft X-ray channel viewing through the plasma edge towards the divertor (Fig. 3(c)) shows no sign of significant ELM activity during the H-mode phase (Fig. 3(b)).

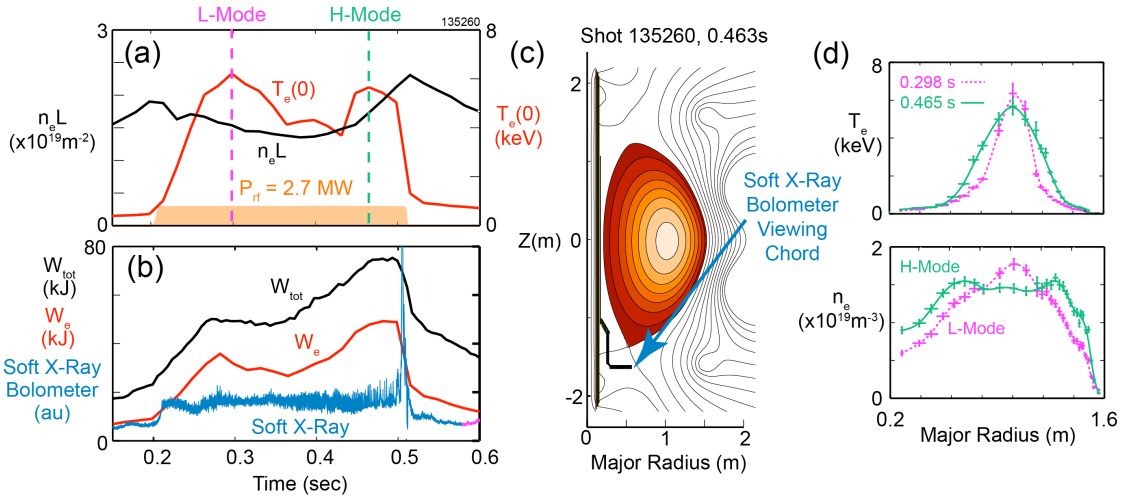

FIGURE 3. Results for a I_p = 650 kA, $B_T(0)$ = 5.5 kG, helium H-mode (shot 135260) heated by 2.7 MW of k_ϕ = -8 m^{-1} RF power. (a) Time evolution of $T_e(0)$ and n_eL and (b) of W_{tot}, W_e and the soft X-ray signal measured along the chord shown in (c). (d) T_e and n_e profiles at 0.298 s (dashed) and 0.465 s (solid).

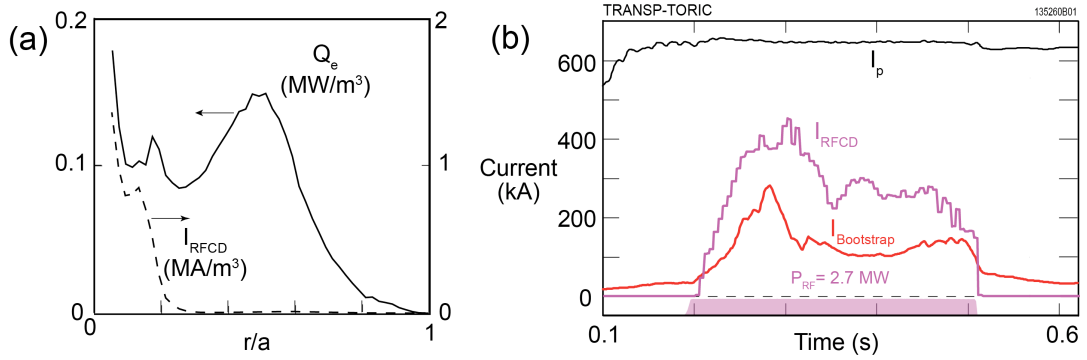

FIGURE 4. (a) RF power deposition to electrons, Q_e,(solid line) and I_{RFCD} (dashed line) calculated by GENRAY-ADJ for P_{RF} = 1 MW for shot 135260 at 0.465 s. (b) Time evolution of I_p, $I_{Bootstrap}$ and I_{RFCD} calculated by TRANSP-TORIC for shot 135260, assuming η_{eff} = 100%.

Figure 4(a) shows RF power deposition to electrons (Q_e) and I_{RFCD} versus r/a for shot 135260 at 0.465 s as calculated with the GENRAY ray tracing code [9] and the ADJ adjoint quasi-linear Fokker-Planck code [10]. Almost all the RF power coupled to the plasma directly heats electrons. Q_e is very broad (solid line), however significant electron trapping constrains I_{RFCD} to a small region near the magnetic axis (dashed line). Figure 4(b) shows the time evolution of I_p, $I_{Bootstrap}$ and I_{RFCD} for shot 135260 calculated by TRANSP-TORIC, assuming η_{eff} = 100%. As mentioned earlier, an approximate value for η_{eff} can be calculated from P_{RF}, ΔW_T and τ. $\Delta W_T \sim$ 25 kJ and

τ ~ 17 ms, yielding η_{eff} ~ 55% for this shot. At 0.465 s, assuming η_{eff} ~ 55%, TRANSP-TORIC predicts I_{RFCD} ~ 140 kA, $I_{Bootstrap}$ ~ 80 kA, and f_{NI} ~ 0.35. ξ_{cd} ~ 0.1 MA/MW, somewhat lower than the ξ_{cd} ~ 0.13 MA/MW predicted by GENRAY-ADJ. These high ξ_{cd} values result from the relatively high $T_e(0)$ and low $n_e(0)$. At 0.298s, when the plasma is still in L-mode, both $I_{Bootstrap}$ and I_{RFCD} are higher, yielding a higher f_{NI} ~ 0.5.

HHFW HEATING OF NBI H-MODE PLASMAS

Improved HHFW coupling to NBI-generated H-modes [4, 5] has resulted in a broad increase in $T_e(R)$ when HHFW heating is applied. Figure 5(a) shows a significant increase in $T_e(R)$, measured by MPTS, when 1.9 MW of k_ϕ = -13 m^{-1} RF power is coupled into an I_p = 900 kA, $B_T(0)$ = 5.5 kG, NBI-generated, deuterium, ELM-free H-mode plasma heated by 2 MW of NBI power (shot 134909), compared to a NBI H-mode (shot 134910) with closely-matched $T_e(R)$ and $n_e(R)$ profiles at the start of the RF heating pulse (0.248 s). A TRANSP-TORIC analysis of these plasmas revealed that about 1 MW of the 1.9 MW launched from the HHFW antenna is damped inside the last closed flux surface (LCFS) [11].

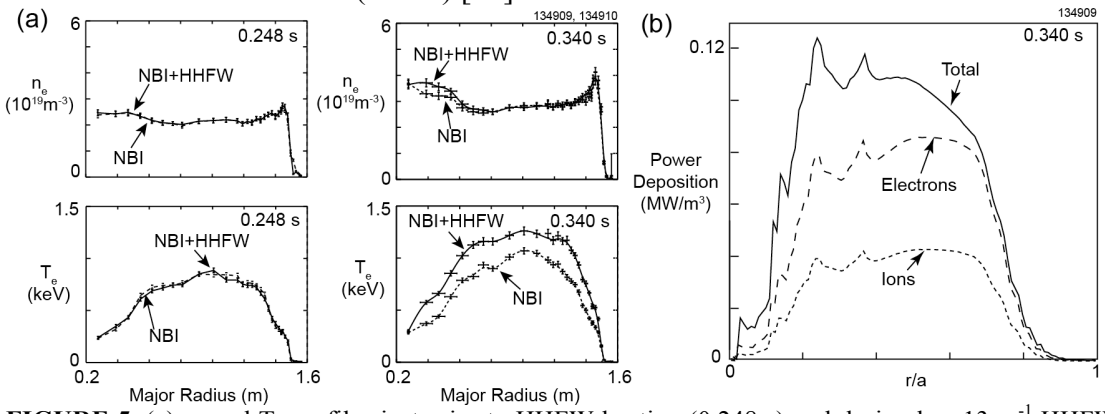

FIGURE 5. (a) n_e and T_e profiles just prior to HHFW heating (0.248 s) and during k_ϕ= 13 m^{-1} HHFW heating (0.340 s) for closely matched I_p = 900 kA, $B_T(0)$ = 5.5 kG, HHFW+ NBI (shot 134909, solid line) and NBI (shot 134910, dashed line) H-mode plasmas. (b) RF power deposition profile versus r/a for P_{RF} = 1 MW, calculated by GENRAY for shot 134909 at 0.340 s.

When HHFW power is coupled into NBI-heated plasmas there is a competition between direct electron heating, via Landau damping and transit-time magnetic pumping, and wave-field acceleration of the NBI-generated fast-ions. GENRAY modeling predicts that of the power damped inside the LCFS in shot 134909, 75% is absorbed directly by electrons and 25% accelerates NBI fast-ions. Figure 5(b) shows the RF deposition profile predicted by GENRAY when 1 MW of k_ϕ = -13 m^{-1} RF power is coupled into shot 134909 at 0.340 s. The RF power deposition is very broad for both the electrons and ions, with very little RF power reaching the axis, as a result I_{RFCD} is only ~3 kA in this case. The CQL3D Fokker-Planck code [12] was used to compute the effect of HHFW wave-field acceleration on the NBI fast ions and the neutron production rate (S_n) in shot 134909. The current version of CQL3D provides a "no loss" calculation (NL), which assumes zero ion Larmor radius and zero banana width, and a "simple-banana-loss" calculation (SBL), which assumes that trapped ions with a banana width plus Larmor radius greater than the distance to the LCFS are lost

in an ion bounce time. CQL3D was run to equilibrium using kinetic profiles and equilibrium data from TRANSP for shot 134909 at 0.340 s. The NL calculation predicts S_n = 2.06 x 10^{14} s^{-1}, much higher than the measured S_n of 1.1±0.2 x 10^{14} s^{-1}, while the SBL calculation predicts S_n = 0.9x10^{14} s^{-1}, about 20% below the measured value. These results are consistent with most of the wave-field accelerated NBI fast-ions being promptly lost from the plasma, as might be expected given that the wave-field acceleration is mostly well off-axis. A fast-ion D-alpha diagnostic (FIDA) [13] measures little or no change in the fast-ion profile for energies between 15 and 90 keV when HHFW heating is applied in this case.

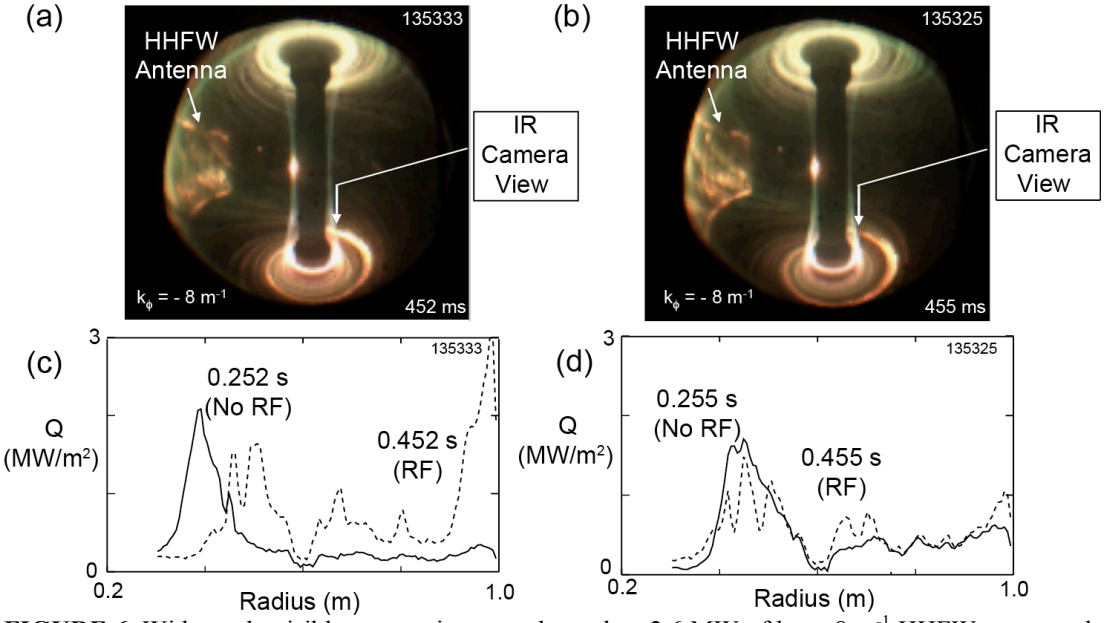

FIGURE 6. Wide angle visible camera images taken when 2.6 MW of k_ϕ = -8 m^{-1} HHFW was coupled into I_p = 0.8 MA, P_{NBI} = 2 MW, H-modes from 0.25 to 0.46 s (a) with $B_T(0)$ = 4.5 kG and (b) with $B_T(0)$ = 5.5 kG. (c) and (d) show plots of the power flux versus major radius on the divertor plate, acquired by a calibrated IR camera viewing the divertor at the location indicated by the arrows in (a) and (b), respectively.

At long toroidal launch wavelengths, HHFW+NBI H-mode plasmas can exhibit a significant RF power flow, along magnetic field lines outside the LCFS, towards the lower divertor. This power flow produces a localized, toroidally elongated, hot region on the divertor plate that is observed to move as the magnetic field pitch is changed [14]. Figure 6 shows visible and calibrated IR camera measurements during two I_p = 0.8 MA HHFW+NBI deuterium H-modes that are heated by 2 MW of NBI power and 2.6 MW of k_ϕ = -8 m^{-1} HHFW power. Figures 6(a) and (c) are for a plasma with $B_T(0)$ = 4.5 kG (shot 135333) and Figs 6(b) and (d) are for a plasma with $B_T(0)$ = 5.5 kG (shot 135325). The visible camera images show emission following the magnetic field from the antenna to the lower divertor plate and an associated toroidally elongated bright region on the lower divertor plate. This bright region moves toroidally when $B_T(0)$ is changed. A calibrated IR camera viewing the divertor at the location indicated by the arrows in Figs 6 (a) and (c) measures the power flux on the divertor plate surface versus major radius (R), as shown in Figs. 6(c) and (d). The solid line is the power flux just before the RF heating is turned on and dashed line is the power flux when the RF has been on for about 200 ms. The power flux peak near

R = 1 m in Fig. 6(c) is due to the RF power flow to the divertor. This peak is much smaller in Fig. 6(d) because the hot region has moved away from the IR camera view.

The presence of ELMs degrades HHFW heating efficiency in both HHFW+NBI and HHFW H-modes, compared to ELM-free H-modes [14]. ELMs directly eject stored energy, as they do during ELMing NBI H-modes that have no HHFW coupled to them, but in addition they can increase the edge density so it exceeds the onset density for perpendicular wave propagation near the antenna [2], leading to increased RF power deposition in the edge and more RF power flow to the lower divertor.

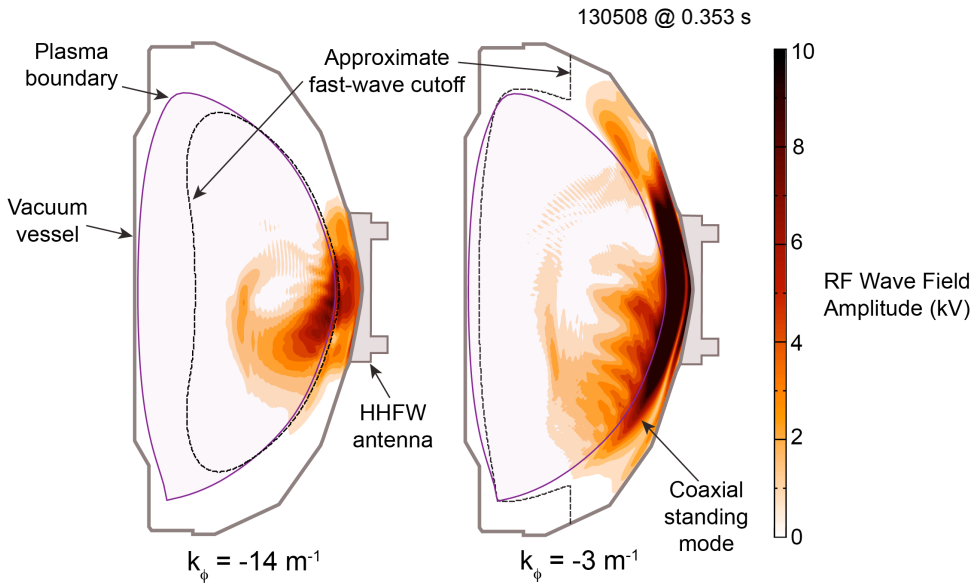

FIGURE 7. AORSA simulated RF wave field amplitudes that includes both the core and scrape-off layer (SOL) outside the LCFS and realistic machine geometry. Simulations are shown for an HHFW + NBI H-mode plasma (shot 130608) which had 2 MW of NBI and 1.9 MW of HHFW power. The left hand simulation is for k_ϕ = -14 m^{-1} heating and the right hand simulation is for k_ϕ = -3 m^{-1} heating. The wave field amplitude color key is shown on the right.

Recently a linear 3-D electromagnetic field solver capable of modeling realistic Tokamak geometries for ion cyclotron range of frequency (ICRF) heating and current drive has been developed [15]. The simulation code is an extension of the AORSA full wave code [16] that includes both the core and scrape-off layer (SOL) outside the LCFS and realistic machine geometry. The code has been used to simulate a NSTX HHFW+NBI H-mode plasma (shot 130608) and the results are summarized in Fig. 7. Simulation results are shown for k_ϕ = -14 m^{-1} and k_ϕ = -3 m^{-1}. At the lowest k_ϕ large amplitude non-propagating coaxial modes form in the SOL, if these large RF wave fields are collisionally damped in the SOL the dissipated power could be significant. In earlier simulations of L-mode HHFW plasmas there are also large amplitude edge-localized, field-aligned, traveling eigenmodes excited just inside the LCFS, however in the cases shown in Fig. 7 these modes appear to have been absorbed due to the high density and temperature just inside the LCFS. These simulation results qualitatively agree with NSTX HHFW+NBI deuterium H-mode data that show decreasing core RF heating efficiency [17] and increasing RF power flow to the lower divertor with decreasing k_ϕ [4]. These simulations support the hypothesis that excitation of coaxial edge modes likely reduce HHFW heating efficiency.

SUMMARY

Improved antenna and plasma conditioning has resulted in the generation of HHFW-only H-mode plasmas that have an ELM-free-like phase with rising stored energy, high $T_e(0)$, and f_{NI} up to 0.65, and it has also enabled a broad increase in $T_e(R)$ when HHFW heating is applied to NBI-generated H-modes. There is a decrease in core heating efficiency and an increase in edge RF power loss when large ELMs are present. In addition, at long launch wavelengths, HHFW+NBI H-mode plasmas can have a significant RF power flow in the SOL that produces a toroidally localized hot region on the lower divertor plate that moves with changes in magnetic field pitch. Full wave modeling, that includes the SOL, predicts modes in the SOL and in the plasma edge that significantly increase in amplitude at long toroidal launch wavelengths, in qualitative agreement with experimental observations. Similar edge/SOL RF power flows to the divertor may also occur in ITER NBI+ICRF H-mode scenarios and may be an important RF power loss mechanism.

ACKNOWLEDGMENTS

The authors wish to acknowledge the support of Drs. Masayuki Ono and Jonathan Menard, the NSTX team and the machine, RF, and neutral beam operations groups. Funding for this research was provided under USDOE Contract No. DE-AC02-09CH11466 and DE-AC05-00OR22725.

REFERENCES

1. M. Ono, *Phys. Plasmas* **2**, 4075 (1995).
2. J. C. Hosea, *et al*., *Phys. Plasmas* **15**, 056104 (2008).
3. C. K. Phillips, *et al.*, *Nucl. Fusion* **49**, 075015 (2009).
4. G. Taylor, *et al*., *Phys. Plasmas* **17**, 056114 (2010).
5. P. M. Ryan, *et al*., this conference.
6. M. Brambilla, *Plasma Phys. Control. Fusion* **44**, 2423 (2002).
7. R. J. Hawryluk, in *Physics of Plasmas Close to Thermonuclear Conditions*, *Proc. of the International School of Plasma Physics*, (Pergamon, Varenna, Italy, 1981), Vol. 1, p. 19.
8. J. C. Hosea, *et al., US-Japan RF Physics Workshop* (February 2011, Toba, Japan)
9. A. P. Smirnov and R.W. Harvey, *Bull. Am. Phys. Soc.* **40**, 1837 (1995).
10. A. P. Smirnov, *et al*., in Proc. 15th Workshop on ECE and ECRH, Edited by J. Lohr, World Scientific, 2009, pp. 301-306.
11. B. P. LeBlanc, *et al*., 23rd IAEA Fusion Energy Conference, Daejon, Korea, paper EXW/P7-12 (October 2010).
12. R. W. Harvey and M. G. McCoy, Proc. of IAEA Tech. Committee on Advances in *Simulation and Modeling of Thermonuclear Plasmas*, Montreal, Quebec (IAEA, Vienna, 1993), p. 489; USDOC NTIS Doc. No. DE93002962.
13. M. Podesta, *et al*., *Rev. Sci. Instrum.* **78**, 10E521 (2008).
14. J. C. Hosea, *et al*., this conference.
15. D. L. Green, *et al*., this conference.
16. E. F. Jaeger, *et al*., *Phys. Rev. Lett.* **90**, 195001 (2003).
17. J. C. Hosea, *et al*., AIP Conf Proc. **1187**, 105 (2009).